

Order parameter fluctuation and ordering competition in $\text{Ba}_{1-x}\text{K}_x\text{Fe}_2\text{As}_2$

Jing Wang,^{1,2} Guo-Zhu Liu,¹ Dmitry V. Efremov,² and Jeroen van den Brink^{2,3}

¹*Department of Modern Physics, University of Science and Technology of China, Hefei, Anhui 230026, P.R. China*

²*Institute for Theoretical Solid State Physics, IFW Dresden, Helmholtzstr. 20, 01069 Dresden, Germany*

³*Institute for Theoretical Physics, TU Dresden, 01069 Dresden, Germany*

The competition among superconductivity, stripe-type magnetic order, and a new type of C_4 symmetric magnetic order in $\text{Ba}_{1-x}\text{K}_x\text{Fe}_2\text{As}_2$ is theoretically studied, focusing on its impact on the global phase diagram. By carrying out a renormalization group analysis of an effective field theory, we obtain the energy-scale dependent flows of all the model parameters, and then apply the results to understand the observed phase diagram. On the basis of the renormalization group analysis, we show that the critical line of nematic order has a negative slope in the superconducting dome and superconductivity is suppressed near the magnetic quantum critical point, which are both consistent with recent experiments. Moreover, we find that, although the observed C_4 symmetric magnetic state could be a charge-spin density wave or a spin-vortex crystal at high temperatures, charge-spin density wave is the only stable C_4 magnetic state in the low-temperature regime. Therefore, ordering competition provides a method to distinguish these two candidate C_4 magnetic states.

PACS numbers: 74.70.Xa, 74.25.Dw, 74.40.Kb, 74.62.-c

I. INTRODUCTION

A universal property shared by most known iron-based superconductors (FeSCs) is the bulk coexistence of two or even more distinct long-range orders [1–12], such as superconductivity, stripe-type spin-density-wave (SDW) order, nematic order, and other possible orders. The competition and coexistence of these orders leads to a very complicated global phase diagram [1–12]. Acquiring a detailed knowledge of the phase diagram is an important step towards a better understanding of FeSCs.

Among the long-range orders competing with superconductivity, a particular role is played by the nematic order, induced by an electronic state that spontaneously breaks the C_4 (tetragonal) symmetry of the system down to a C_2 (orthogonal) symmetry. Extensive experiments have confirmed that nematic order exists in almost all FeSCs [2–5, 13–17]. In most cases, the nematic order sets in at a temperature T_n slightly higher than the critical temperature of magnetic order T_m [4, 6, 10, 18, 19]. Usually, the magnetic order is generated by a stripe-type SDW, and possesses two characteristic vectors $\mathbf{Q}_X = (\pi, 0)$ and $\mathbf{Q}_Y = (0, \pi)$ in the Brillouin zone of the iron square lattice, which relate to the spin operator $S(\mathbf{r})$ in the form $S(\mathbf{r}) = M_{X,Y}e^{i\mathbf{Q}_{X,Y}\cdot\mathbf{r}}$ [12, 20]. This stripe SDW breaks the discrete lattice rotational symmetry by selecting out only one of the two characteristic vectors \mathbf{Q}_X and \mathbf{Q}_Y , preserving the C_2 symmetry [6, 8, 10, 12]. Because the nematic order and SDW order coexist over a large part of the global phase diagram, it is widely believed [3–6, 8–12] that the nematic order is actually induced by the fluctuation of magnetic order.

It was unexpected that experiments had found a new type of C_4 symmetric magnetic order that preserves the tetragonal symmetry in a number of hole-doped FeSCs, including $\text{Ba}(\text{Fe}_{1-x}\text{Mn}_x)_2\text{As}_2$ [21], $\text{Ba}_{1-x}\text{Na}_x\text{Fe}_2\text{As}_2$ [22, 23], $\text{Sr}_{1-x}\text{K}_x\text{Fe}_2\text{As}_2$ [24], and $\text{Ba}_{1-x}\text{K}_x\text{Fe}_2\text{As}_2$ [25–28]. This C_4 magnetic state is characterized by biaxial mag-

netic orders [29–33], and the corresponding spin operator is given by $S(\mathbf{r}) = M_X e^{i\mathbf{Q}_X\cdot\mathbf{r}} + M_Y e^{i\mathbf{Q}_Y\cdot\mathbf{r}}$ [33, 34]. It has been suggested that this double- \mathbf{Q} magnetic state has two possible realizations [29–33, 35]: a charge-spin density wave (CSDW) in which M_X and M_Y are collinear; a spin-vortex crystal (SVC) in which M_X and M_Y are orthogonal. Since the largest value of T_c of FeSCs is observed at the proximity of tetragonal C_4 magnetic order [22, 26], there might exist a quantum critical point (QCP) at certain doping x_c in the superconducting (SC) dome [33]. After its discovery, the double- \mathbf{Q} structured C_4 SDW state has stimulated a variety of experimental [21, 22, 24–27] and theoretical works [29–34, 36–39].

In this paper, we consider the effects caused by the competition of superconductivity with both stripe-type C_2 symmetric and C_4 symmetric magnetic orders in a hole-doped FeSC $\text{Ba}_{1-x}\text{K}_x\text{Fe}_2\text{As}_2$ [21, 22, 24–27]. Recently, Böhmer *et al.* [26] have experimentally investigated the global phase diagram of $\text{Ba}_{1-x}\text{K}_x\text{Fe}_2\text{As}_2$, and identified five distinct thermodynamically stable ordered phases, which are schematically shown in Fig. 1. One can see that the critical line for the nematic order displays a rather complicated dependence on doping x and temperature T : it decreases with growing x at high T , bends backwards to lower x slightly above T_c , and eventually exhibits a negative slope after penetrating into the SC dome. In the narrow doping region in which the nematic critical line has a positive slope, T_c is moderately suppressed. Close to the putative magnetic QCP, represented by x_2 in Fig. 1, there appears on the phase diagram a region that manifests C_4 symmetric SDW state, which occupies part of the usual C_2 symmetric SDW phase and coexists with superconductivity below T_c . In principle, the experimentally observed C_4 SDW state might be a CSDW or SVC type state, which needs to be clarified theoretically.

Instead of trying to explain the entire phase diagram observed in Ref. [26], we perform a more moderate task

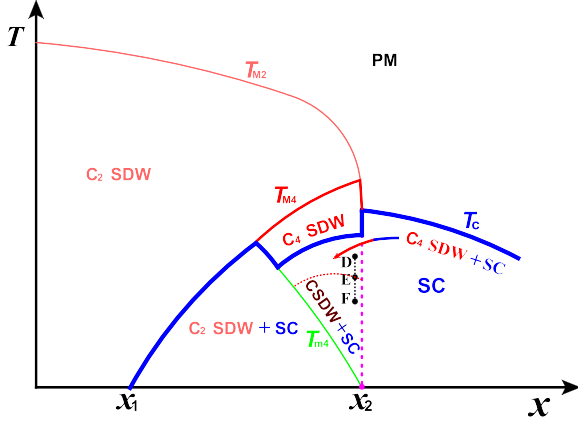


FIG. 1: (Color online) Schematic global phase diagram of $\text{Ba}_{1-x}\text{K}_x\text{Fe}_2\text{As}_2$ on (x, T) plane [26], with x_1 and x_2 being two QCPs. T_{M2} is the transition line between paramagnetic (PM) and C_2 -symmetric magnetic phases, and T_c is the SC transition line. T_{M4} is the transition line between C_2 - and C_4 -symmetric magnetic phases above T_c , whereas T_{m4} denotes such a transition line inside the SC dome. The observed C_4 symmetric SDW state could be either CSDW or SVC. Distinct phases are distinguished by different values of the model parameters [33, 34] defined in Eq. (4): (i) $g < 0$ and $w = 0$, the system is in PM phase; (ii) $g > \max(0, -w)$ represents the C_2 symmetric SDW phase (with nematic order); (iii) C_4 symmetric magnetic state is of SVC-type if $g < 0$ and $w > 0$, and CSDW-type if $g < -w$ and $w < 0$.

in this work. In particular, we will concentrate on the narrow doping region surrounding the magnetic QCP x_2 inside the SC dome and endeavor to answer the following questions. How to determine whether the observed C_4 magnetic state is of CSDW or SVC type? What is the scenario that leads to suppresses superconductivity near the magnetic QCP? Why does the nematic critical line display a negative, rather than positive, slope in the SC dome? We will address these issues by investigating the impact of order competition in the low- T regime.

We study an effective field theory that can be used to describe the low-energy physics of $\text{Ba}_{1-x}\text{K}_x\text{Fe}_2\text{As}_2$ and other analogous FeSCs [12, 18–20, 30, 35]. When the parameters used in this model take different values, the system might be in the paramagnetic state, C_4 tetragonal SDW state, or C_2 symmetric magnetic state. The fluctuations of the associated order parameters and the competition between distinct orders can qualitatively alter the magnitudes and even the sign of the model parameters, which would drive phase transitions and reshape the global phase diagram. After analyzing the competition between nematic and SC orders by means of renormalization group (RG) method, we find that the slope of nematic critical line is always negative in the SC dome. We also extract the T -dependence of superfluid density from RG results, which clearly shows that superconductivity is suppressed near magnetic QCP. Moreover, we infer from the RG results that, although CSDW and SVC state are both possible in the high- T regime, the CSDW state is

the only stable one in the low- T regime, which provides a promising way to specify the true nature of the observed C_4 symmetric SDW state.

The rest of paper is organized as follows. In Sec. II, we present the effective field theory for the ordering competition and then derive the coupled flow equations of all the model parameters by performing perturbative RG calculations. In Sec. III, we numerically solve the equations and apply the RG solutions to understand several important features of the global phase diagram of $\text{Ba}_{1-x}\text{K}_x\text{Fe}_2\text{As}_2$ observed in recent experiments. The Sec. IV is followed to present some discussions. In Sec. V, we present a brief summary of the results.

II. EFFECTIVE THEORY AND RG ANALYSIS

Many of the basic properties of $\text{Ba}_{1-x}\text{K}_x\text{Fe}_2\text{As}_2$ can be described by a three-band model that contains one hole pocket at the center of Brillouin zone $\mathbf{Q}_\Gamma = (0, 0)$ and two electron pockets centered at two specific momenta $\mathbf{Q}_X = (\pi, 0)$ and $\mathbf{Q}_Y = (0, \pi)$ [12, 18–20, 30, 33–35]. The microscopic model is written as [12, 19]

$$H = \sum_{\mathbf{k}, i \in (X, Y, \Gamma)} \varepsilon_{\mathbf{k}, i} c_{\mathbf{k}\sigma, i}^\dagger c_{\mathbf{k}\sigma, i} + H_4, \quad (1)$$

with the interacting term H_4 is given by

$$H_4 = \sum_{\mathbf{k}, i \in (X, Y)} \frac{U_3}{2} \left(c_{\mathbf{k}\alpha, \Gamma}^\dagger c_{\mathbf{k}\gamma, \Gamma}^\dagger c_{\mathbf{k}\delta, i} c_{\mathbf{k}\beta, i} + \text{h.c.} \right) \delta_{\alpha\beta} \delta_{\gamma\delta} \\ + \sum_{\mathbf{k}, i \in (X, Y)} U_1 c_{\mathbf{k}\alpha, \Gamma}^\dagger c_{\mathbf{k}\gamma, \Gamma}^\dagger c_{\mathbf{k}\delta, i} c_{\mathbf{k}\beta, \Gamma} \delta_{\alpha\beta} \delta_{\gamma\delta}. \quad (2)$$

Here, U_1 and U_3 represent density-density interaction and the pair hopping interaction, respectively. They are responsible for the formation of superconductivity and SDW state [19, 40, 41]. The magnetic structure can be described by two order parameters \mathbf{M}_X and \mathbf{M}_Y , corresponding to the ordering vectors $\mathbf{Q}_X = (\pi, 0)$ and $\mathbf{Q}_Y = (0, \pi)$, which are defined as $\mathbf{M}_j = \sum_{\mathbf{k}} c_{\Gamma, \mathbf{k}\alpha}^\dagger \vec{\sigma}_{\alpha\beta} c_{j, \mathbf{k}+\mathbf{Q}_j\beta}$ with $j = X, Y$ [18, 19, 42–44]. Both the C_2 and C_4 symmetric magnetic orders are modeled by the following Ginzburg-Landau free energy [33, 34]

$$f[\mathbf{M}_X, \mathbf{M}_Y] = a_m(\mathbf{M}_X^2 + \mathbf{M}_Y^2) + \frac{u}{2}(\mathbf{M}_X^2 + \mathbf{M}_Y^2)^2 \\ - \frac{g}{2}(\mathbf{M}_X^2 - \mathbf{M}_Y^2)^2 + 2w(\mathbf{M}_X \cdot \mathbf{M}_Y)^2.$$

As illustrated in Ref. [33], the term $2w(\mathbf{M}_X \cdot \mathbf{M}_Y)^2$ can be rewritten by using an identity:

$$(\mathbf{M}_X \cdot \mathbf{M}_Y)^2 = \frac{1}{4}(\mathbf{M}_X^2 + \mathbf{M}_Y^2)^2 - \frac{1}{4}(\mathbf{M}_X^2 - \mathbf{M}_Y^2)^2 \\ - (\mathbf{M}_X \times \mathbf{M}_Y)^2. \quad (3)$$

Upon carrying out a Hubbard-Stratonovich transformation followed by an integration over all the fermionic degrees of freedom, one can obtain an effective field theory

[19, 33] for the interplay of SDW magnetic and SC orders in the vicinity of magnetic QCP:

$$\begin{aligned}\mathcal{L} = & \frac{1}{2}(\partial_\mu M_X)^2 + \frac{1}{2}(\partial_\mu M_Y)^2 + a_m(M_X^2 + M_Y^2) \\ & + \frac{(u+w)}{2}(M_X^2 + M_Y^2)^2 - \frac{(g+w)}{2}(M_X^2 - M_Y^2)^2 \\ & + \partial_\mu \Delta^\dagger \partial_\mu \Delta + a_s \Delta^2(k) + \frac{u_s}{2} \Delta^4(k) + \frac{\varphi^2}{2w} + \mathcal{L}_A \\ & - 2\varphi M_X M_Y + \lambda(M_X^2 + M_Y^2)\Delta^2 + \lambda_{\Delta A} \Delta^2 A^2, \quad (4)\end{aligned}$$

where Δ is the SC order parameter. Here we use a positive parameter λ to characterize the repulsive interaction (competition) between SC and magnetic orders. In order to evaluate the superfluid density, we have introduced a gauge potential \mathbf{A} via the standard minimal coupling [45] with $\mathcal{L}_A = -\frac{1}{4}(\partial_\mu A_\nu - \partial_\nu A_\mu)^2$. This model contains eight fundamental parameters $a_m, a_s, u_s, w, u, g, \lambda$, and $\lambda_{\Delta A}$, which are constants at the mean-field level, but all become cutoff dependent due to interactions.

The transition lines for SDW and SC orders are determined by taking $a_m = 0$ and $a_s = 0$ respectively. For s^{+-} -wave superconductors, we employ the relationship $\Delta_\Gamma = -\sqrt{2}\Delta_{X,Y} = \Delta$ [8, 12, 19]. An Ising-type nematic order is induced by the magnetic order, and represented by a term of the form $M_X^2 - M_Y^2$ [8, 12, 18]. The property of C_4 magnetic order is determined by the parameter w [33, 34]. In the SC dome, the SC order parameter develops a nonzero mean value, i.e., $\langle \Delta \rangle = V_0 = \sqrt{-a_s/u_s}$ near the magnetic QCP x_2 .

The effective model (4) displays different states when the model parameters take various values [33, 34]. (i) If $g < 0$ and $w = 0$, the effective model is in paramagnetic (PM) phase; (ii) The case of $g > \max(0, -w)$ corresponds to the C_2 SDW phase (with nematic order); (iii) The C_4 symmetric magnetic state is of SVC-type if $g < 0$ and $w > 0$, and CSDW-type if $g < -w$ and $w < 0$. Once some of these parameters are altered by external forces, such as doping, magnetic field, and pressure, the system would

undergo transitions between distinct phases. However, the quantum fluctuations of order parameters and the interaction between different order parameters can also lead to remarkable changes of model parameters, and as such drive phase transitions. In the next section, we will study the RG flows of these parameters and examine how they are influenced by order parameter fluctuation and ordering competition. The main results are schematically illuminated in Fig. 1 and the detailed derivations and discussions are given in the following.

To proceed, we perform a RG analysis of the effective theory (4). Our focus is on the behavior of the system at low T and in the vicinity of magnetic QCP. Within this region, the quantum fluctuations of SC order parameter can result in drastic effects even in the SC phase. For the complex SC order parameter $\Delta(\mathbf{r})$, there are two sorts of fluctuations [46–53], namely the phase fluctuation and amplitude fluctuation. The former fluctuation is gapless and corresponds to the Nambu-Goldstone mode induced by continuous gauge symmetry breaking. This mode does not play any role in the SC state because it is absorbed by the vector gauge boson via the Anderson-Higgs mechanism. The latter one, known as Higgs mode in a locally gauge invariant superconductor, is found by both theoretical and experimental works to result in observable effects [46–53], and hence should be seriously considered [54, 55]. In order to capture the quantum fluctuation of SC order parameter around its mean value $\langle \Delta \rangle$, we define two new fields h and η by [54, 55]

$$\Delta = V_0 + \frac{1}{\sqrt{2}}(h + i\eta), \quad (5)$$

where $\langle h \rangle = \langle \eta \rangle = 0$. The fields h and η stand for the Higgs mode and Nambu-Goldstone mode, respectively. We substitute Eq. (5) into the effective Lagrangian density \mathcal{L} (4), and obtain the following new effective Lagrangian density:

$$\begin{aligned}\mathcal{L}_{\text{eff}} = & \frac{1}{2}(\partial_\mu M_X)^2 + \alpha_X M_X^2 + \frac{\beta_X}{2} M_X^4 + \frac{1}{2}(\partial_\mu M_Y)^2 + \alpha_Y M_Y^2 + \frac{\beta_Y}{2} M_Y^4 + \frac{1}{2}(\partial_\mu h)^2 + \alpha_h h^2 + \frac{\beta_h}{2} h^4 + \gamma_h h^3 \\ & + \left(\mathcal{L}_A + \frac{\alpha_A}{2} A^2 \right) + \alpha_\varphi \varphi^2 + \gamma_{\varphi XY} \varphi M_X M_Y + \gamma_{X^2 h} M_X^2 h + \gamma_{Y^2 h} M_Y^2 h + \gamma_{hA^2} h A^2 + \lambda_{Xh} M_X^2 h^2 \\ & + \lambda_{Yh} M_Y^2 h^2 + \lambda_{XY} M_X^2 M_Y^2 + \lambda_{hA} h^2 A^2.\end{aligned} \quad (6)$$

The gapless Nambu-Goldstone mode η naturally disappears after invoking the Anderson-Higgs mechanism. However, the Higgs mode h remains in the above effective model, and couple directly to the magnetic order parameters $M_{X,Y}$ and also to vector potential A . The originally massless gauge field A acquires a finite mass α_A after absorbing η . Moreover, in the above Lagrangian density we have introduced a number of new parameters that are related to the model parameters defined in (4) by the following relations:

$$\begin{aligned}\alpha_X = \alpha_Y \equiv & a_m - \frac{\lambda a_s}{u_s}, \quad \alpha_A \equiv \frac{-2\lambda_{\Delta A} a_s}{u_s}, \quad \alpha_h \equiv -a_s, \quad \alpha_\varphi \equiv \frac{1}{2w}, \quad \beta_X = \beta_Y \equiv u - g, \quad \beta_h \equiv \frac{u_s}{4}, \\ \gamma_h \equiv & \frac{\sqrt{-2a_s u_s}}{2}, \quad \gamma_{hA^2} \equiv \sqrt{\frac{-2\lambda_{\Delta A}^2 a_s}{u_s}}, \quad \gamma_{\varphi XY} \equiv -2, \quad \gamma_{X^2 h} = \gamma_{Y^2 h} \equiv \sqrt{\frac{-2\lambda^2 a_s}{u_s}}, \\ \lambda_{XY} \equiv & u + g + 2w, \quad \lambda_{hA} \equiv \frac{\lambda_{\Delta A}}{2}, \quad \lambda_{Xh} = \lambda_{Yh} \equiv \frac{\lambda}{2}.\end{aligned} \quad (7)$$

Using these relations, we can derive the flow equations of fundamental parameters by calculating the effective parameters α_X , α_h , α_φ , β_X , β_h , λ_{XY} , λ_{Xh} , and λ_{hA} . By performing perturbative expansion in powers of small coupling parameters [56] and utilizing \dot{u} to denote the derivative of u with respect to the varying length scale l , we arrive at the following flow equations with the help of the identities given by Eq. (7) [55]:

$$\begin{aligned}
\dot{a}_m &= 2 \left(a_m - \frac{\lambda a_s}{u_s} \right) + \frac{1}{4\pi^2} \left\{ \frac{\lambda}{2} (1 + 2a_s) + \frac{8\lambda^2 a_s^2}{u_s} + \left[1 - 2 \left(a_m - \frac{\lambda a_s}{u_s} \right) \right] \left[2(2u - g) + \frac{4\lambda^2 a_s}{u_s} \right] \right\} \\
&\quad + \left(\frac{\lambda}{u_s} \dot{a}_s + \frac{a_s}{u_s} \dot{\lambda} - \frac{a_s \lambda}{u_s^2} \dot{u}_s \right), \\
\dot{a}_s &= 2a_s - \frac{1}{12\pi^2} \left\{ \frac{27a_s u_s}{2} (1 + 4a_s) + \frac{12a_s \lambda^2}{u_s} \left[1 - 4 \left(a_m - \frac{a_s \lambda}{u_s} \right) \right] + 3\lambda \left[1 - 2 \left(a_m - \frac{a_s \lambda}{u_s} \right) \right] \right. \\
&\quad \left. + \frac{9u_s}{4} (1 + 2a_s) + 3\lambda_{\Delta A} \left(1 + \frac{2a_s \lambda_{\Delta A}}{u_s} \right) + \frac{32a_s \lambda_{\Delta A}^2}{u_s} \left(1 + \frac{4a_s \lambda_{\Delta A}}{u_s} \right) \right\}, \\
\dot{u}_s &= u_s + \frac{1}{\pi^2} \left\{ -\frac{9u_s^2}{4} (4a_s + 1) + 2\lambda^2 \left[4 \left(a_m - \frac{a_s \lambda}{u_s} \right) - 1 \right] + 54a_s u_s^2 (1 + 6a_s) - \frac{4\lambda_{\Delta A}^2}{3} \left(\frac{4a_s \lambda_{\Delta A}}{u_s} + 1 \right) \right. \\
&\quad \left. + \frac{32a_s \lambda^3}{u_s} \left(1 + \frac{6a_s \lambda}{u_s} \right) + \frac{11072a_s \lambda_{\Delta A}^3}{35u_s} \left(1 + \frac{6a_s \lambda_{\Delta A}}{u_s} \right) \right\}, \\
\dot{u} &= u + w + \frac{1}{2\pi^2} \left\{ [9(u - g)^2 + 3(u + g + 2w)(u - g) + 5(u + g + 2w)^2 + 12w(u - g)] \left[4 \left(a_m - \frac{a_s \lambda}{u_s} \right) - 1 \right] \right. \\
&\quad - \frac{3\lambda^2}{8} (4a_s + 1) + \frac{24a_s \lambda^2 (u - g)}{u_s} \left[1 - 2 \left(2 \left(a_m - \frac{a_s \lambda}{u_s} \right) - a_s \right) \right] + 4w(u + g + 2w) \left[4 \left(a_m - \frac{a_s \lambda}{u_s} \right) - 1 \right] \\
&\quad \left. + \frac{8a_s \lambda^2 (u + g + 2w)}{u_s} \left[1 - 4 \left(a_m - \frac{a_s \lambda}{u_s} \right) + 2a_s \right] + \frac{4a_s \lambda^3}{u_s} \left[1 - 2 \left(a_m - \frac{a_s \lambda}{u_s} \right) + 4a_s \right] \right\} - \dot{w}, \\
\dot{g} &= g + w - \frac{1}{2\pi^2} \left\{ [9(u - g)^2 - 3(u + g + 2w)(u - g) - 3(u + g + 2w)^2 - 12w(u - g)] \left[4 \left(a_m - \frac{a_s \lambda}{u_s} \right) - 1 \right] \right. \\
&\quad - \frac{\lambda^2}{8} (4a_s + 1) + \frac{24a_s \lambda^2 (u - g)}{u_s} \left[1 - 2 \left(2 \left(a_m - \frac{a_s \lambda}{u_s} \right) - a_s \right) \right] + 4w(u + g + 2w) \left[4 \left(a_m - \frac{a_s \lambda}{u_s} \right) - 1 \right] \\
&\quad \left. - \frac{8a_s \lambda^2 (u + g + 2w)}{u_s} \left[1 - 4 \left(a_m - \frac{a_s \lambda}{u_s} \right) + 2a_s \right] + \frac{4a_s \lambda^3}{u_s} \left[1 - 2 \left(a_m - \frac{a_s \lambda}{u_s} \right) + 4a_s \right] \right\} - \dot{w}, \\
\dot{\lambda} &= \lambda + \frac{1}{\pi^2} \left\{ \frac{4a_s \lambda^3}{u_s} \left[1 - 4 \left(a_m - \frac{a_s \lambda}{u_s} \right) + 2a_s \right] + \lambda(2u - g + 3w) \left[4 \left(a_m - \frac{a_s \lambda}{u_s} \right) - 1 \right] \right. \\
&\quad + \frac{16a_s \lambda^2 (2u - g + w)}{u_s} \left[1 - 6 \left(a_m - \frac{a_s \lambda}{u_s} \right) \right] + 6a_s \lambda^2 \left[1 - 2 \left(a_m - \frac{a_s \lambda}{u_s} \right) + 4a_s \right] \\
&\quad \left. - \frac{3u_s \lambda}{8} (4a_s + 1) + 2\lambda^2 \left[2 \left(a_m - \frac{a_s \lambda}{u_s} \right) - 2a_s - 1 \right] + 9a_s u_s \lambda (1 + 6a_s) \right\}, \\
\dot{\lambda}_{\Delta A} &= \lambda_{\Delta A} + \frac{1}{3\pi^2} \left\{ 27a_s u_s \lambda_{\Delta A} (1 + 6a_s) + \frac{4\lambda_{\Delta A}^2 (16a_s \lambda_{\Delta A} - 3u_s)}{u_s} \left[1 + 2a_s \left(1 + \frac{2\lambda_{\Delta A}}{u_s} \right) \right] \right. \\
&\quad \left. - \frac{9u_s \lambda_{\Delta A}}{8} (4a_s + 1) + 36a_s \lambda_{\Delta A}^2 \left[1 + 2a_s \left(2 + \frac{\lambda_{\Delta A}}{u_s} \right) \right] \right\}, \\
\dot{w} &= \frac{w^2}{\pi^2} \left[1 - 4 \left(a_m - \frac{\lambda a_s}{u_s} \right) \right].
\end{aligned} \tag{8}$$

III. COMPARISON WITH EXPERIMENTS

In this section, we will compare the RG results with recent experiments. We first numerically solve the self-consistently coupled RG equations, and then manage to understand a number of important features observed by Böhmer *et al.* in $\text{Ba}_{1-x}\text{K}_x\text{Fe}_2\text{As}_2$ [26]. We are particularly interested in the doping dependence of nematic critical line in the SC dome, the suppression of superconductivity observed at the magnetic QCP, and the nature of the observed C_4 symmetric magnetic order, which will

be studied one by one based on the RG solutions.

As can be seen from the phase diagram presented in Fig. 1, the magnetic and SC orders are assumed to coexist over a finite region, with x_2 being the magnetic QCP. Such a coexistence can be realized if the bare values of model parameters satisfy the constraint [19, 20, 57–60] $\lambda < \sqrt{u_s[(u + w) - (g + w)]} = \sqrt{u_s(u - g)}$. For simplicity, we will only consider the low- T region in the close vicinity of the magnetic QCP inside the SC dome. In addition, the external field A is assumed to be weak, but the basic conclusion does not depend on this assumption.

A. Slope of nematic critical line in SC dome

The nematic line is not shown apparently in Fig. 1. However, the C_2 magnetic phase is always accompanied (even preempted) by a nematic phase with a critical temperature T_n higher than that of C_2 magnetic order [6, 8, 10, 19]. Hence T_{m4} is also a nematic critical line.

A known fact is that a long-range order can always be destroyed by thermal fluctuation at sufficiently high T . In a system containing two or more distinct orders, the competition between these orders might destroy some specific order at very low T . As a result, the critical line on the (x, T) phase diagram for this specific order has a positive slope in the low- T region, which is often called back-bending behavior. Interestingly, such back-bending behavior has been observed in some high- T_c cuprate superconductor [61–63] and FeSCs [64]. In cuprate $\text{Bi}_2\text{Sr}_2\text{CaCu}_2\text{O}_{8+\delta}$, a pseudogap exists above T_c on the (x, T) phase diagram. This pseudogap decreases rapidly with growing doping x , so its critical line exhibits a negative slope above T_c . However, after entering into the SC dome, the critical line for pseudogap was found to bend backwards to lower doping, and thus displays a positive slope in the low- T region [61–63]. A similar behavior was also observed in $\text{Ba}(\text{Fe}_{1-x}\text{Co}_x)_2\text{As}_2$ by Nandi *et al.* [64]. In this case, it is the nematic order that is in strong competition with SC order. The nematic critical line has a negative slope on (x, T) phase diagram above T_c , but displays a positive slope below T_c [64]. A common feature observed in these two compounds is that the critical line for the order competing with superconductivity has a positive slope in the low- T region. While a convincing theoretic explanation for the back-bending of pseudogap critical line in $\text{Bi}_2\text{Sr}_2\text{CaCu}_2\text{O}_{8+\delta}$ is lacking, a recent RG work reproduced the back-bending of nematic critical line by studying the competition between nematic and SC orders in $\text{Ba}(\text{Fe}_{1-x}\text{Co}_x)_2\text{As}_2$ [65]. Different from $\text{Ba}(\text{Fe}_{1-x}\text{Co}_x)_2\text{As}_2$, the nematic critical line has a negative slope in the SC dome of $\text{Ba}_{1-x}\text{K}_x\text{Fe}_2\text{As}_2$ [26] despite the presence of ordering competition.

In $\text{Ba}(\text{Fe}_{1-x}\text{Co}_x)_2\text{As}_2$, there is only C_2 symmetric magnetic order, induced by a stripe-type SDW state. As discussed in Ref. [19], the existence of nematic order is tuned by the quadratic term $-g(M_X^2 - M_Y^2)^2$. The system can stay either in the PM phase, or in one of the M_X and M_Y magnetically ordered phases. The former case corresponds to a state in which $g < 0$ and no nematic order exists. In the latter case, $g > 0$ and hence the system exhibits a nematic order. Both of these two possibilities can be realized at low T . When the competition between nematic and SC orders is sufficiently strong, it is in principle possible for the nematic order to be suppressed in the low- T region, leading to a positive slope of nematic critical line in the SC dome [65].

We now use the RG solutions to judge whether the nematic critical line has a positive or negative slope in the SC dome of $\text{Ba}_{1-x}\text{K}_x\text{Fe}_2\text{As}_2$. In the effective field model given by Eq. (4), the relation between g and w

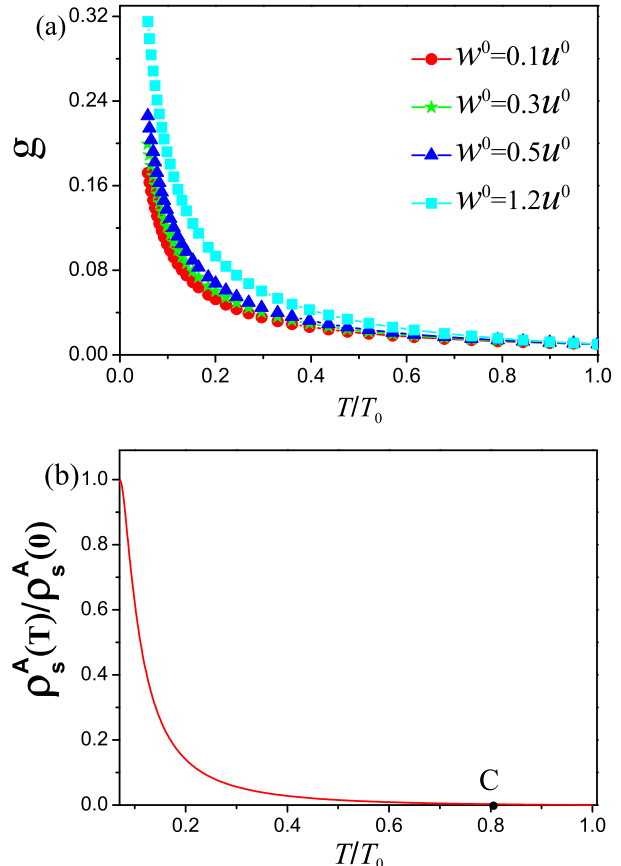


FIG. 2: (Color online) (a) T -dependence of parameter g at several different values of w_0 . Calculations confirm that the positive parameter g never becomes negative as T decreases. (b) T -dependence of $\rho_s^A(T)/\rho_s^A(0)$. The quantity $\rho_s^A(T=0)$ is temperature independent at sufficiently low temperatures in the absence of ordering competition. It is apparent that $\rho_s^A(T)$ vanishes at certain point C, where $T \approx 0.8T_0$.

determines whether the nematic order is present or not. As pointed out previously in Refs. [10, 18, 65], when $g > \max(0, -w)$, only one of the two order parameters M_X and M_Y develops a finite mean value due to tetragonal symmetry breaking, which is a clear signature for the existence of a nematic order. On the other hand, we have $\langle M_X \rangle = \langle M_Y \rangle$ if $g < \max(0, -w)$, which implies the absence of nematic order [10, 18, 65]. This property will be used to judge whether the nematic critical line bends back.

To examine how the relation between g and w varies with decreasing T , we have solved the RG equations and obtained its dependence on the running length scale l . To be specific, we have chosen the following bare values of model parameters: $a_s^0 = -0.001$, $u^0 = 0.05$, $u_s^0 = 0.01$, $g^0 = 0.01$, $\lambda^0 = 0.01$, $\lambda_{\Delta A}^0 = 1.0 \times 10^{-8}$. We consider several representative values of w^0 : $w^0 = 0.1u^0$, $0.3u^0$, $0.5u^0$, and $1.2u^0$. The l -dependence of these parameters can be easily converted to a T -dependence by utilizing

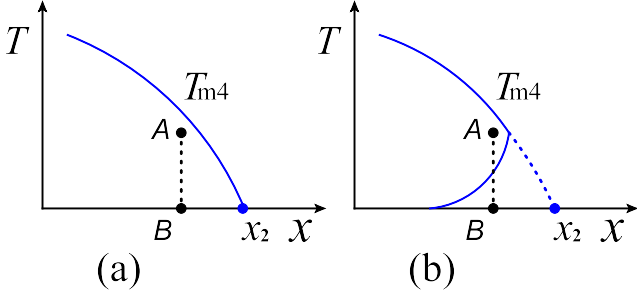


FIG. 3: Two possibilities about the slopes of the nematic transition lines.

the transformation [65–67] $T = T_0 e^{-l}$, where T_0 is some reference temperature smaller than T_c . The numerical results are presented in Fig. 2(a). We now determine whether the nematic state becomes a non-nematic state as T is lowered down to zero on the basis of these results.

There are in principle two possibilities about the slopes of nematic transition line T_{m4} , as schematically shown in Fig. 3. We consider an arbitrary point A lying slightly below the transition line T_{m4} . At point A , the system is in the nematic state with $g > \max(0, -w)$. We then lower T along the route $A \rightarrow B$. If the inequality $g > \max(0, -w)$ is always satisfied as $T \rightarrow 0$ along $A \rightarrow B$, the system is always in the nematic state and the slope of the transition line T_{m4} is negative. This corresponds to the case represented by Fig. 3(a). In contrast, if the condition $g > \max(0, -w)$ is violated as T is reduced to certain value, the second possibility shown in Fig. 3(b) occurs. In this case, the nematic state becomes non-nematic once again and the slope of transition line becomes positive at lower temperatures, exhibiting back-bending behavior. The numerical results of Eq. (8) informs that the ratio $g/|w| \gg 1$ for various values of l , wherein w may be both positive and negative (it is negative for the curve shown in Fig. 4). From the asymptotic behaviors of $g(l)$ presented in Fig. 2(a) and $g(l)/|w(l)|$ presented in Fig. 4, we infer that the inequality $g > \max(0, -w)$ remains true as $T \rightarrow 0$ if it is satisfied at the starting point A . This clearly indicates that the nematic transition line T_{m4} has a negative slope inside the SC dome and never bends backwards, which is well consistent with the observed phase diagram [26].

B. Suppression of superconductivity due to ordering competition

We now verify whether superconductivity is suppressed by ordering competition in the vicinity of the magnetic QCP. To this end, we will compute the superfluid density after taking into account the ordering competition among nematic (C_2 SDW), C_4 SDW and SC orders. The T -dependence of superfluid density $\rho_s(T)$ is computed based on the l -dependence of parameter $\alpha_A \equiv \alpha_A(l)$ [66, 67], which is extracted from the coupled flow equa-

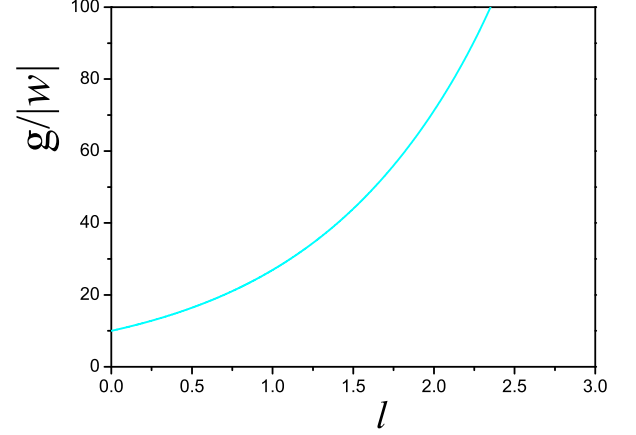


FIG. 4: (Color online) The evolutions of $g/|w|$ at some representative initial values of parameters: $a_s^0 = -0.001$, $u_s^0 = 0.05$, $u^0 = 0.01$, $g^0 = 0.01$, $\lambda^0 = 0.01$, and $\lambda_{\Delta A}^0 = 1.0 \times 10^{-8}$. The basic conclusion is independent of these initial values.

tion (8) and hence captures the ordering competition. The superfluid density of superconductor has the generic form $\rho_s(T) = \rho_s^A(T) - \rho_n(T)$, where $\rho_s^A(T)$ can be evaluated by virtue of the formula $\rho_s^A(T) \propto \alpha_A(T)$ with $\alpha_A(T)$ being the mass for vector potential \mathbf{A} generated via Anderson-Higgs mechanism [45] and $\rho_n(T)$ is the density of thermally excited normal (non-SC) fermionic quasiparticles.

In this work, we consider only the competition between distinct order parameters and neglect the contribution of the normal component, i.e. $\rho_n(T) \ll \rho_s^A(T)$, which is possible for the $T \ll T_c$, focusing on how superfluid density is modified by ordering competition. To determine the impact of ordering competition, we suppose a specific temperature T_0 as a reference, and then examine how superfluid density ρ_s varies as a function of the ratio T/T_0 . We assume that T_0 is well below T_c so that the normal fermionic quasiparticles can nearly be neglected and hence $\rho_s(T) \sim \rho_s^A(T)$. From the results displayed in Fig. 2(b), we can see that $\rho_s^A(T)$ is strongly dependent of T in the presence of ordering competition and decreases rapidly as T/T_0 grows. It is thus clear that the superfluid density is strongly suppressed by ordering competition and approximately goes to zero in the vicinity of the point C , where $T \approx 0.8T_0$.

We then consider the impact of ordering competition on T_c . The value of T_c can be determined by solving the equation $\rho_s(T_c) = \rho_s^A(T) - \rho_n(T_c) = 0$. Although the contribution $\rho_n(T)$ is not known, we can still infer that T_c is suppressed by ordering competition because ρ_s is significantly reduced. As shown in Fig. 2(b), $\rho_s(T)$ vanishes at certain point with $T < T_0$ ($T \approx 0.8T_0$). This conclusion is well consistent with recent experiment [26], in which a considerable drop of T_c is observed near the putative magnetic QCP. In an improved theoretic treatment, one would compute $\rho_n(T)$ by incorporating the contribution

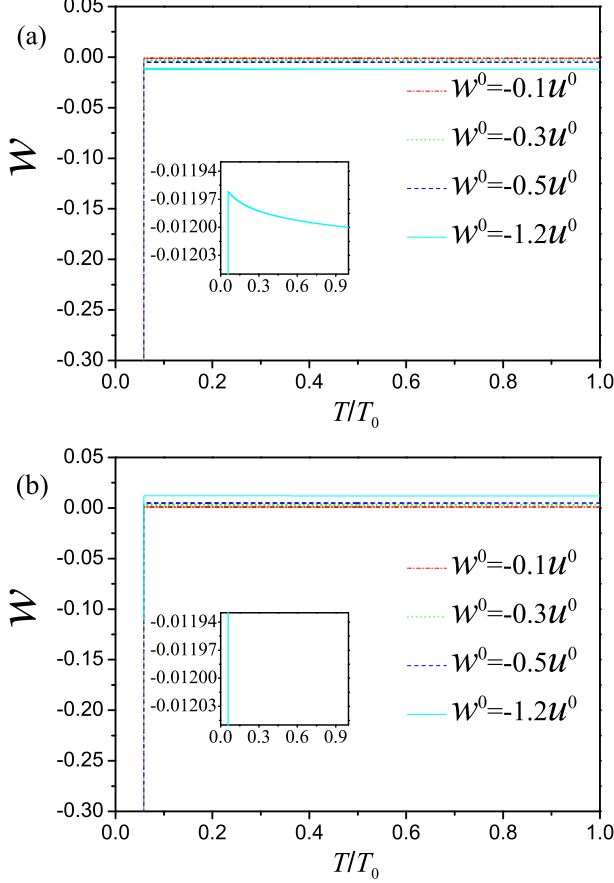


FIG. 5: (Color online) T -dependence of parameter w obtained at given bare values of dimensionless parameters: $a_s^0 = -0.001$, $u_s^0 = 0.05$, $u^0 = 0.01$, $g^0 = -0.01$, $\lambda^0 = 0.01$, and $\lambda_{\Delta A}^0 = 1.0 \times 10^{-8}$. The main conclusion is independent of these bare values. The parameter w is not very sensitive to the change of T , so we provide two insets to show more clearly how w varies as T is decreasing. (a) Starting point is CSDW-type C_4 state with $w^0 < 0$; (b) Starting point is SVC-type C_4 state with $w^0 > 0$.

of fermionic quasiparticles. Notice that these quasiparticles are not free, but couple strongly to the SDW order parameter at the magnetic QCP [68–74]. Usually, this coupling tends to excite more fermionic quasiparticles out of the SC condensate, which further suppresses the superfluid density and reduces T_c [68–74].

C. C_4 symmetric magnetic order

We finally turn to analyze the property of C_4 symmetric magnetic state. To uncover the effects caused by ordering competition, we consider the evolution of the system along the route $D \rightarrow E \rightarrow F$, shown in Fig. 1, and examine how g and w vary along this route.

Eq. (4) clearly shows that w is associated with the quadratic term of C_4 SDW order parameter [33, 34]. In

analogy to the nematic transition, the sign of w determines which sort of C_4 SDW order, either SVC or CSDW, is realized [10, 18, 33, 34, 65]. In particular, a C_4 SVC order is generated for $g < 0$ and $w > 0$, whereas $g < -w$ and $w < 0$ implies the occurrence of a C_4 CSDW order [10, 18, 33, 34, 65]. By paralleling the analysis made for nematic critical line, we convert the l -dependence of w using the transformation $T = T_0 e^{-l}$. If one assumes that w is negative at the starting point D , which amounts to supposing the system is in the CSDW-type C_4 magnetic state, it remains negative as T decreases down to the F point, as can be clearly seen from Fig. 5(a). This result implies that CSDW state is stable in the low- T region. On the other hand, if one starts from a positive w , corresponding to a SVC-type C_4 magnetic state, we show in Fig. 5(b) that w eventually becomes negative at some critical T , which can be identified as the E point. It follows that the SVC state is unstable in the low- T region, and that the CSDW state is more favorable.

We conclude from the above analysis that, although in principle either SVC or CSDW type C_4 state could be realized in the high- T region, the CSDW-type C_4 state is the only stable one in the low- T region. In a recent work, Christensen *et al.* [75] have suggested the spin-orbit coupling gives rise to the CSDW-type C_4 SDW. Additionally, Hoyer *et al.* [34] have studied the disorder effects and demonstrated that impurity scattering favors CSDW over SVC. Here, we provide a different approach to determine the nature of C_4 symmetric magnetic order. Moreover, the sudden drop of w at certain critical energy scale usually indicates the happening of a first-order transition, which is qualitatively consistent with recent experiments [26].

IV. COMPARISON TO $\text{Ba}(\text{Fe}_{1-x}\text{Co}_x)_2\text{As}_2$

We now compare the present RG results with a previous work [65], which investigated the impact of ordering competition on the global phase diagram of $\text{Ba}(\text{Fe}_{1-x}\text{Co}_x)_2\text{As}_2$. Both $\text{Ba}(\text{Fe}_{1-x}\text{Co}_x)_2\text{As}_2$ and $\text{Ba}_{1-x}\text{K}_x\text{Fe}_2\text{As}_2$ belong to the 122 family of FeSCs, and display a complicated phase diagram. A common feature is that, over a large part of their phase diagrams, superconductivity coexists and competes with a SDW type magnetic order and a nematic order. The ordering competition and its effects on the phase diagram can be described by deriving an effective low-energy field theory which is supposed to contain several distinct order parameters [12, 19, 33, 34]. Such an effective theory is expected to be as general as possible, and applicable in $\text{Ba}(\text{Fe}_{1-x}\text{Co}_x)_2\text{As}_2$, $\text{Ba}_{1-x}\text{K}_x\text{Fe}_2\text{As}_2$, and other similar 122 FeSCs.

However, there are some important differences between the compounds $\text{Ba}(\text{Fe}_{1-x}\text{Co}_x)_2\text{As}_2$ and $\text{Ba}_{1-x}\text{K}_x\text{Fe}_2\text{As}_2$. In $\text{Ba}(\text{Fe}_{1-x}\text{Co}_x)_2\text{As}_2$, there is only a C_2 symmetric stripe-type SDW order. In contrast, there are both C_2 and C_4 symmetric magnetic states in $\text{Ba}_{1-x}\text{K}_x\text{Fe}_2\text{As}_2$

and a number of other hole-doped 122 FeSCs [21–28]. Moreover, the nematic transition line exhibits completely different doping dependence in the SC dome of these two FeSCs: it has a positive slope inside the SC dome of $\text{Ba}(\text{Fe}_{1-x}\text{Co}_x)_2\text{As}_2$ [64], but a negative slope inside the SC dome of $\text{Ba}_{1-x}\text{K}_x\text{Fe}_2\text{As}_2$ [26].

To capture both the similarity and difference, the model of $\text{Ba}_{1-x}\text{K}_x\text{Fe}_2\text{As}_2$ should be formally analogous but not identical to that of $\text{Ba}(\text{Fe}_{1-x}\text{Co}_x)_2\text{As}_2$ [65]. It was suggested in Refs.[33, 34] that the C_4 symmetric magnetic order that emerges in $\text{Ba}_{1-x}\text{K}_x\text{Fe}_2\text{As}_2$ can be described by introducing a new term $-(\mathbf{M}_X \times \mathbf{M}_Y)^2$. As shown previously in Ref.[65], in the absence of this term, ordering competition gives rise to the suppression of superconductivity and in particular the positive slope of nematic transition line in the SC dome, which are in good agreement with experiments performed in $\text{Ba}(\text{Fe}_{1-x}\text{Co}_x)_2\text{As}_2$ [64]. In the current work, we have demonstrated through RG calculations that, adding the above new term leads to the suppression of superconductivity near the magnetic QCP and also the negative slope of nematic transition line in the SC dome of $\text{Ba}_{1-x}\text{K}_x\text{Fe}_2\text{As}_2$, which is qualitatively consistent with recent experiments [25–28]. Furthermore, our RG analysis revealed that the CSDW-type C_4 magnetic state is more favorable than the SVC-type C_4 magnetic state, and hence can be used to determine the nature of C_4 magnetic state observed in $\text{Ba}_{1-x}\text{K}_x\text{Fe}_2\text{As}_2$ [26]. It is therefore clear that the effective model of $\text{Ba}(\text{Fe}_{1-x}\text{Co}_x)_2\text{As}_2$ can be properly modified to describe $\text{Ba}_{1-x}\text{K}_x\text{Fe}_2\text{As}_2$, and that the same perturbative RG scheme used in Ref.[65] and here can be applied to account for both the similarity and difference between $\text{Ba}(\text{Fe}_{1-x}\text{Co}_x)_2\text{As}_2$ and $\text{Ba}_{1-x}\text{K}_x\text{Fe}_2\text{As}_2$.

V. SUMMARY AND DISCUSSION

In summary, we have studied the impact of the competition between superconductivity and C_2 and C_4 symmetric magnetic orders in a hole-doped FeSC $\text{Ba}_{1-x}\text{K}_x\text{Fe}_2\text{As}_2$. After performing a detailed RG analysis within an effective field theory, we have reproduced a number of interesting features of the global phase diagram. In particular, our RG analysis have showed that the order parameter fluctuation and ordering competition lead to moderate suppression of superconductivity near the magnetic QCP, maintain the negative slope of nematic critical line in the SC dome, and also sort out the CSDW-type C_4 magnetic order as the more stable state than a SVC-type C_4 magnetic order in the low- T regime. All these theoretic results are well consistent with the recent experiments of Ref. [26], and schematically summarized in Fig. 1.

Our RG calculations are confined to the small region surrounding the magnetic QCP in the SC dome. To gain a better knowledge of the entire phase diagram, it is necessary to consider the non-SC phase above T_c . A salient

feature observed in Ref. [26] is the back-bending behavior of a critical line between nematic (C_2 SDW) to pure C_4 SDW orders, namely T_{M4} , which turns out to be induced by the emergence of C_4 symmetric magnetic order. The transition line T_{M4} exists well above T_c , thus there is no SC order and the competition between SC and magnetic order parameters is unlikely to be important. It turns out that the underlying mechanism for the back-bending behavior of T_{M4} is entirely different from that is used to account for the slope of T_{m4} in the SC dome. We believe that an essential role is played by elementary fermionic degrees of freedom, which are strongly suppressed below T_c by the SC gap but should be present above T_c . The inter-fermion interaction is expected to be responsible for the transition between C_4 and C_2 symmetric magnetic states. This problem is made more complicated by the uncertainty of the nature of C_4 symmetric magnetic order. In the SC dome below T_c , ordering competition lifts the degeneracy between CSDW and SVC states at low energies, and chooses CSDW as the true ground state. However, order competition is much less important above T_c . It remains unclear whether the CSDW or SVC state is realized in the region between T_{M4} and T_c . The microscopic mechanism for the back-bending behavior of T_{M4} could be properly understood only after the nature of C_4 symmetric magnetic order is identified, which is subject to future research.

In this paper, we have considered only one specific compound $\text{Ba}_{1-x}\text{K}_x\text{Fe}_2\text{As}_2$. Recent experiments of Hardy *et al.* [26] provided a clear and detailed global phase diagram of $\text{Ba}_{1-x}\text{K}_x\text{Fe}_2\text{As}_2$, which gives us a good opportunity to directly compare our RG results with experimental results. Apart from $\text{Ba}_{1-x}\text{K}_x\text{Fe}_2\text{As}_2$, the C_4 symmetric magnetic order also exists in a number of other hole-doped FeSCs, including $\text{Ba}(\text{Fe}_{1-x}\text{Mn}_x)_2\text{As}_2$ [21], $\text{Ba}_{1-x}\text{Na}_x\text{Fe}_2\text{As}_2$ [22, 23], and $\text{Sr}_{1-x}\text{K}_x\text{Fe}_2\text{As}_2$ [24]. It should be possible to generalize our RG approach to study the global phase diagrams of these three FeSCs. However, there might be important difference between $\text{Ba}_{1-x}\text{K}_x\text{Fe}_2\text{As}_2$ and these FeSCs. In that case, the effective field-theoretic model given by Eq. (4) needs to be properly modified. Once the modified effective model is specified, it is straightforward to carry out RG calculations, just as what we have done in this work.

VI. ACKNOWLEDGEMENTS

J.W. and G.Z.L. acknowledge the financial support from the National Natural Science Foundation of China under Grants 11504360, 11274286, and 11574285. J.W. is also partly supported by the China Postdoctoral Science Foundation under Grants 2015T80655 and 2014M560510, the Fundamental Research Funds for the Central Universities (P. R. China) under Grant WK2030040074, and the Program of Study Abroad for Young Scholar sponsored by CSC (China Scholarship Council). D.V.E. and J.v.d.B. would like to acknowledge the financial support

provided by the German Research Foundation (Deutsche Forschungsgemeinschaft) through priority program SPP

1458. J.v.d.B is also supported by SFB 1143 of the Deutsche Forschungsgemeinschaft.

-
- [1] D. S. Inosov, J. T. Park, P. Bourges, D. L. Sun, Y. Sidis, A. Schneidewind, K. Hradil, D. Haug, C. T. Lin, B. Keimer and V. Hinkov, *Nat. Phys.* **6**, 178 (2009).
 - [2] J. Paglione and R. L. Greene, *Nat. Phys.* **6**, 645 (2010).
 - [3] G. R. Stewart, *Rev. Mod. Phys.* **83**, 1589 (2011).
 - [4] I. R. Fisher, L. Degiorgi, and Z. X. Shen, *Rep. Prog. Phys.* **74**, 124506 (2011).
 - [5] P. J. Hirschfeld, M. M. Korshunov, and I. I. Mazin, *Rep. Prog. Phys.* **74**, 124508 (2011).
 - [6] D. N. Basov and A. V. Chubukov, *Nat. Phys.* **7**, 272 (2011).
 - [7] P. Dai, J. Hu, and E. Dagotto, *Nat. Phys.* **8**, 709 (2012).
 - [8] A. V. Chubukov, *Annu. Rev. Condens. Matter Phys.* **3**, 57 (2012).
 - [9] E. Dagotto, *Rev. Mod. Phys.* **85**, 849 (2013).
 - [10] R. M. Fernandes, A. V. Chubukov, and J. Schmalian, *Nat. Phys.* **10**, 97 (2014).
 - [11] P. C. Dai, *Rev. Mod. Phys.* **87**, 855 (2015).
 - [12] R. M. Fernandes and A. V. Chubukov, *Rep. Prog. Phys.* **80**, 014503 (2017).
 - [13] M. G. Kim, R. M. Fernandes, A. Kreyssig, J. W. Kim, A. Thaler, S. L. Bud'ko, P. C. Canfield, R. J. McQueeney, J. Schmalian, and A. I. Goldman, *Phys. Rev. B* **83**, 134522 (2011).
 - [14] C. R. Rotundu and R. J. Birgeneau, *Phys. Rev. B* **84**, 092501 (2011).
 - [15] S. Avci, O. Chmaissem, D. Y. Chung, S. Rosenkranz, E. A. Goremychkin, J. P. Castellan, I. S. Todorov, J. A. Schlueter, H. Claus, A. Daoud-Aladine, D. D. Khalyavin, M. G. Kanatzidis, and R. Osborn, *Phys. Rev. B* **85**, 184507 (2012).
 - [16] S. Kasahara, H. J. Shi, K. Hashimoto, S. Tonegawa, Y. Mizukami, T. Shibauchi, K. Sugimoto, T. Fukuda, T. Terashima, A. H. Nevidomskyy and Y. Matsuda, *Nature* **486**, 382 (2012).
 - [17] R. Zhou, Z. Li, J. Yang, D. L. Sun, C. T. Lin, and G.-Q. Zheng, *Nature Comm.* **4**, 2265 (2013).
 - [18] R. M. Fernandes, A. V. Chubukov, J. Knolle, I. Eremin, and J. Schmalian, *Phys. Rev. B* **85**, 024534 (2012).
 - [19] R. M. Fernandes, S. Maiti, P. Wölfle, and A. V. Chubukov, *Phys. Rev. Lett.* **111**, 057001 (2013).
 - [20] R. M. Fernandes, D. K. Pratt, W. Tian, J. Zarestky, A. Kreyssig, S. Nandi, M. G. Kim, A. Thaler, N. Ni, P. C. Canfield, R. J. McQueeney, J. Schmalian, and A. I. Goldman, *Phys. Rev. B* **81**, 140501(R) (2010).
 - [21] M. G. Kim, A. Kreyssig, A. Thaler, D. K. Pratt, W. Tian, J. L. Zarestky, M. A. Green, S. L. Bud'ko, P. C. Canfield, R. J. McQueeney, and A. I. Goldman, *Phys. Rev. B* **82**, 220503(R) (2010).
 - [22] S. Avci, O. Chmaissem, J. M. Allred, S. Rosenkranz, I. Eremin, A. V. Chubukov, D. E. Bulgari, D. Y. Chung, M. G. Kanatzidis, J.-P. Castellan, J. A. Schlueter, H. Claus, D. D. Khalyavin, P. Manuel, A. Daoud-Aladine, and R. Osborn, *Nat. Commun.* **5**, 3845 (2014).
 - [23] L. Wang, F. Hardy, A. E. Böhrer, T. Wolf, P. Schweiss, and C. Meingast, *Phys. Rev. B* **93**, 014514 (2016).
 - [24] J. M. Allred, K. M. Taddei, D. E. Bugaris, M. J. Krogstad, S. H. Lapidus, D. Y. Chung, H. Claus, M. G. Kanatzidis, D. E. Brown, J. Kang, R.M. Fernandes, I. Eremin, S. Rosenkranz, O. Chmaissem, and R. Osborn, *Nat. Phys.* **10**, 1038 (2016).
 - [25] E. Hassinger, G. Gredat, F. Valade, S. René de Cotret, A. Juneau-Fecteau, J.-Ph. Reid, H. Kim, M. A. Tanatar, R. Prozorov, B. Shen, H.-H. Wen, N. Doiron-Leyraud, and Louis Taillefer, *Phys. Rev. B* **86**, 140502 (2012).
 - [26] A. E. Böhrer, F. Hardy, L. Wang, T. Wolf, P. Schweiss, and C. Meingast, *Nat. Commun.* **6**, 7911 (2015).
 - [27] J. M. Allred, S. Avci, D. Y. Chung, H. Claus, D. D. Khalyavin, P. Manuel, K. M. Taddei, M. G. Kanatzidis, S. Rosenkranz, R. Osborn, and O. Chmaissem, *Phys. Rev. B* **92**, 094515 (2015).
 - [28] E. Hassinger, G. Gredat, F. Valade, S. R. de Cotret, O. CyrChoiniere, A. Juneau-Fecteau, J.-Ph. Reid, M. H. Kim, A. Tanatar, R. Prozorov, B. Shen, H.-H. Wen, N. Doiron-Leyraud, and L. Taillefer, *Phys. Rev. B* **93**, 144401 (2016).
 - [29] J. Lorenzana, G. Seibold, C. Ortix, and M. Grilli, *Phys. Rev. Lett.* **101**, 186402 (2008).
 - [30] I. Eremin and A. V. Chubukov, *Phys. Rev. B* **81**, 024511 (2010).
 - [31] P. M. R. Brydon, J. Schmiedt, and C. Timm, *Phys. Rev. B* **84**, 214510 (2010).
 - [32] G. Giovannetti, C. Ortix, M. Marsman, M. Capone, J. van den Brink, and J. Lorenzana, *Nat. Comm.* **2**, 398 (2011).
 - [33] R. M. Fernandes, S. A. Kivelson, and E. Berg, *Phys. Rev. B* **93**, 014511 (2016).
 - [34] M. Hoyer, R. M. Fernandes, A. Levchenko, and J. Schmalian, *Phys. Rev. B* **93**, 144414 (2016).
 - [35] J. Knolle, I. Eremin, A. V. Chubukov, and R. Moessner, *Phys. Rev. B* **81**, 140506(R) (2010).
 - [36] M. N. Gastiasoro and B. M. Andersen, *Phys. Rev. B* **92**, 140506(R) (2015).
 - [37] D. D. Scherer, I. Eremin, and B. M. Andersen, *Phys. Rev. B* **94**, 180405(R) (2016).
 - [38] J. Kang and Z. Tesanovic, *Phys. Rev. B* **83**, 020505 (2011).
 - [39] M. N. Gastiasoro and B. M. Andersen, *Phys. Rev. Lett.* **113**, 067002 (2014).
 - [40] A. V. Chubukov, D. V. Efremov, and I. Eremin, *Phys. Rev. B* **78**, 134512 (2008).
 - [41] S. Maiti and A. V. Chubukov, *Phys. Rev. B* **82**, 214515 (2010).
 - [42] C. Fang, H. Yao, W.-F. Tsai, J. P. Hu, and S.A. Kivelson, *Phys. Rev. B* **77**, 224509 (2008).
 - [43] C. Xu, M. Muller, and S. Sachdev, *Phys. Rev. B* **78**, 020501(R) (2008).
 - [44] R. M. Fernandes, L. H. VanBebber, S. Bhattacharya, P. Chandra, V. Keppens, D. Mandrus, M. A. McGuire, B. C. Sales, A. S. Sefat, and J. Schmalian, *Phys. Rev. Lett.* **105**, 157003 (2010).
 - [45] B. I. Halperin, T. C. Lubensky, and S.-K. Ma, *Phys. Rev. Lett.* **32**, 292 (1974).
 - [46] C. M. Varma, *J. Low Temp. Phys.* **126**, 901 (2002).

- [47] W. Zwerger, Phys. Rev. Lett. **92**, 027203 (2004).
- [48] D. Podolsky, A. Auerbach, and D. P. Arovas, Phys. Rev. B **84**, 174522 (2011).
- [49] D. Podolsky and S. Sachdev, Phys. Rev. B **86**, 054508 (2012).
- [50] L. Pollet and N. Prokof'ev, Phys. Rev. Lett. **109**, 010401 (2012).
- [51] M. Endres, T. Fukuhara, D. Pekker, M. Cheneau, P. Schaub, C. Gross, E. Demler, S. Kuhr, and I. Bloch, Nature **487**, 454 (2012).
- [52] Y. Barlas and C. M. Varma, Phys. Rev. B **87**, 054503 (2013).
- [53] D. Pekker and C. M. Varma, Annu. Rev. Condens. Matter Phys. **6**, 269 (2015).
- [54] H. Kleinert and F. S. Nogueira, Nucl. Phys. B **651**, 361 (2003).
- [55] J. Wang and G.-Z. Liu, Phys. Rev. D **90**, 125015 (2014).
- [56] R. Shankar, Rev. Mod. Phys. **66**, 129 (1994).
- [57] J.-H. She, J. Zaanen, A. R. Bishop, and A. V. Balatsky, Phys. Rev. B **82**, 165128 (2010).
- [58] A. B. Vorontsov, M. G. Vavilov, and A. V. Chubukov, Phys. Rev. B **79**, 060508(R) (2009); A. B. Vorontsov, M. G. Vavilov, and A. V. Chubukov, Phys. Rev. B **81**, 174538 (2010).
- [59] R. M. Fernandes and J. Schmalian, Phys. Rev. B **82**, 014521 (2010).
- [60] J. Wang and G.-Z. Liu, New J. Phys. **15**, 073039 (2013).
- [61] I. M. Vishik, M. Hashimoto, R.-H. He, W.-S. Lee, F. Schmitt, D. Lu, R. G. Moore, C. Zhang, W. Meevasana, T. Sasagawa, S. Uchida, K. Fujita, S. Ishida, M. Ishikado, Y. Yoshida, H. Eisaki, Z. Hussain, T. P. Devereaux, and Z.-X. Shen, Proc. Natl. Acad. Sci. USA **109**, 18332 (2012).
- [62] M. Hashimoto, E. A. Nowadnick, R.-H. He, I. M. Vishik, B. Moritz, Y. He, K. Tanaka, R. G. Moore, D. Lu, Y. Yoshida, M. Ishikado, T. Sasagawa, K. Fujita, S. Ishida, S. Uchida, H. Eisaki, Z. Hussain, T. P. Devereaux, and Z.-X. Shen, Nat. Mat. **14**, 37 (2015).
- [63] M. Hashimoto, I. M. Vishik, R.-H. He, T. P. Devereaux, and Z.-X. Shen, Nat. Phys. **10**, 483 (2014).
- [64] S. Nandi, M. G. Kim, A. Kreyssig, R. M. Fernandes, D. K. Pratt, A. Thaler, N. Ni, S. L. Bud'ko, P. C. Canfield, J. Schmalian, R. J. McQueeney, and A. I. Goldman, Phys. Rev. Lett. **104**, 057006 (2010).
- [65] J. Wang and G.-Z. Liu, Phys. Rev. B **92**, 184510 (2015).
- [66] Y. Huh and S. Sachdev, Phys. Rev. B **78**, 064512 (2008).
- [67] J.-H. She, M. J. Lawler, and E.-A. Kim, Phys. Rev. B **92**, 035112 (2015).
- [68] G.-Z. Liu, J.-R. Wang, and J. Wang, Phys. Rev. B **85**, 174525 (2012).
- [69] Y. Wang and A. V. Chubukov, Phys. Rev. Lett. **110**, 127001 (2013).
- [70] A. Levchenko, M. G. Vavilov, M. Khodas, and A. V. Chubukov, Phys. Rev. Lett. **110**, 177003 (2013).
- [71] D. Chowdhury, B. Swingle, E. Berg, S. Sachdev, Phys. Rev. Lett. **111**, 157004 (2013).
- [72] T. Nomoto, H. Ikeda, Phys. Rev. Lett. **111**, 167001 (2013).
- [73] J. Kang, X.-Y. Wang, A. V. Chubukov, and R. M. Fernandes, Phys. Rev. B **91**, 121104(R) (2015).
- [74] A. V. Chubukov, I. Eremin, and D. V. Efremov, Phys. Rev. B **93**, 174516 (2016).
- [75] M. H. Christensen, J. Kang, B. M. Andersen, I. Eremin, and R. M. Fernandes, Phys. Rev. B **92**, 214509 (2015).